Summer 8-9-2017

Seismic Facies Classification of an Intraslope Minibasin in The Keathley Canyon, Northern Gulf of Mexico

Lamine Meroudj
University of New Orleans, merlam2007@yahoo.fr

Seismic Facies Classification of an Intraslope Minibasin in The Keathley Canyon, Northern Gulf of Mexico.

A thesis

Submitted to the Graduate Faculty of the
University of New Orleans
In partial fulfillment of the
requirements for the degree of

Master of Science
In
Earth and Environmental Science
Geophysics

By

Lamine Meroudj

B.S. University of Constantine, 2008

August 2017

Acknowledgment

The author is grateful to PGS (petroleum Geo-services) for donating the 3D seismic Data; without it this work would not have been done. I would like also to extend a large amount of gratitude to Schlumberger and Ocean for providing Petrel and necessary plug-ins along with technical support.

Table of Contents

List of Figures iii
List of Tables iii
List of Abbreviation iii
Abstract iii
Introduction 1
Data 2
Methods 4
Seismic Attributes Analysis 6
Attributes Crossploting 9
Correlation Analysis 10
Principle Component Analysis 11
Data Training and Classification 12
Facies Succession 13
Application to an Intraslope Minibasin in the Keathley Canyon 19
Conclusion 20
Recommendations 20
References 21
Vita 24

List of Figures

Figure 1: Base map showing the wide azimuth towed streamer (WATS) survey completed by PGS, highlighted by dark blue; the black box approximately outlines the study area. The data is located on the outer continental shelf within the tabular salt and minibasin province of the Gulf of Mexico (GOM) (https://www.pgs.com/data-library/north-and-south-america/gulf-of-mexico/crystal-wats-a--b/). 3

Figure 2: Workflow for unsupervised ANN. 5

Figure 3: Inline 2387 crosssection through the mininbasin illustrating (a) original seismic section, (b) RMS amplitude, (C) envelope, (D) dominant frequency. Important reflectors such as the sea floor and top of salt are annotated. Color scale bars are displayed at the lower right corner of each section. 8

Figure 4: Crossplot of envelope versus dominant frequency. There are 2 major clusters with some outliers. The points in the second cluster are more spread out then the first cluster that has a spiking character. Therefore, both attributes are selected for facies classification. 9

Figure 5: Crossplot of RMS amplitude versus dominant frequency. There are 2 major clusters with some outliers. The clusters show similar characteristics as in envelope versus dominant frequency. Therefore, both attributes are selected for facies classification. 10

Figure 6: Crossplot of envelope versus RMS amplitude. The plot shows a high correlation because both attributes are related to the energy content of the seismic trace, and they both emphasize the high-energy content of the seismic data. 10

Figure 7: Graphic representation of (a) Principle Components Eigenvalues, (b) Contribution pie chart. The first principle component has the highest eigenvalue which contributes about two thirds. The second principle component contributes about one third. The third principle component has the least contribution. 12

Figure 8: The attributes used in the classification are: RMS amplitude, envelope and dominant frequency. The competitive learning algorithm self organizes the user defined number of classes. In the learning process, the central points of each class are distributed randomly, and then adjusted to fit the center of each class. There were 20 iterations with the maximum error of 10%. 13

Figure 9: Sand beds were picked at well kc102 using the gamma ray log; the sand line was at 50 API. The blue facies coincide with intervals that contain sand. 14

Figure 10: Cross section showing the different facies classes. dark blue class represent the most sand-rich facies. Light blue represents shale-rich facies. Purple is associated with salt. 15

Figure 11: (A) sketch that simplifies the main parameters and terminology for simple model. stratal point

termination location are the result of the interplay between volume of sedimentation and volume of subsidence: if volume of sedimentation exceeds the volume made through subsidence, there would be an onlap at the basin flank (B); if opposite, an offlap would be observed (C) (from Zoltan et al., 2015). 16

Figure 12: (a) Original cross section through the minibasin with seismic facies delineated. (b) correspondent cross section through ANN facies classification cube. The stacking pattern of seismic facies is like those found by modeling. Ct, Cb and bypass facies are present except for offlaping facies that are hard to observe on seismic section. On the classification section, the dark blue facies are associated with sand rich intervals which coincide with Cb facies on seismic section. 18

List of Tables

Table 1: Correlation analysis result. Desired attributes for classification are those with correlation coefficient lower than 0.5 which means there is less the 50% similarity between them. Highly correlated attributes with correlation coefficient greater than 0.5 are represented by red sells which are again RMS amplitude and envelope. 11

Table 2: Principle components with their eigenvalues and overall contributions. These principle components are eigenvectors that best represent the data matrices, and that are scaled by eigenvalues. The components are classified from highest to lowest depending on their contribution. 12

List of Abbreviations

Artificial Neural Network .....ANN
Bottom of Salt.....BOS
Correlation Analysis .....CA
Formation Top .....FT
Keathley Canyon .....KC
Principal Component Analysis .....PCA
Petroleum Geo-Services.....PGS
Sea Floor .....SF
Top of Salt ..... TOS
Wide Azimuth Towed Streamer ..... WATS
Wave Equation Migrated .....WEM

Abstract

This work examines several volume attributes extracted from 3D seismic data with the goal of seismic facies classification and lithology prediction in intraslope minibasins. The study area is in the Keathley Canyon protraction (KC), within the middle slope of the Northern Gulf of Mexico (GOM). It lays within the tabular salt and minibasins province downdip of the main Pliocene and Pleistocene deltaic depocenters. Interaction between sedimentation and mobile salt substrate lead to the emergence of many stratigraphic patterns in the intraslope minibasins. Interest in subsalt formations left above salt formations poorly logged. Facies classification using Artificial Neural Network (ANN) was applied in those poorly logged areas. The resultant facies classes were calibrated and used to predict the lithology of the recognized facies patterns in an intraslope minibasin, away from well control. Three types of facies classes were identified: Convergent thinning, convergent baselaping and bypassing. The convergent baselaping are found to be the most sand rich among all other facies.

Keywords: Keathley Canyon, Gulf of Mexico; facies classification; seismic attributes intraslope minibasins; salt tectonics.

Introduction

The slope of the Gulf of Mexico is characterized by numerous salt withdrawal minibasins (Diegel et al., 1995). These minibasins are circular to ecliptic depressions in the local sea floor topography, resulting from differential loading of a deforming salt substrate by clastic sediments (Prather et al., 1998; Hudec and Jackson, 2007; Hudec et al., 2009; Pilcher et al., 2011; Peel, 2014). Sand transported by turbidity currents and other sediment gravity flows can be preferentially trapped within these basins which makes them a significant hydrocarbon reservoir, especially for those that are deeply buried (Mahaffie, 1994; Prather et al., 1998; Kendrick, 2000; Booth et al., 2003). The stratigraphy of intraslope minibasins has been studied previously by Satterfield and Behrens (1990), Boyd et al. (1993), McGee et al. (1993), Steffens (1993), Lee et al. (1996). Many of these works focused on depositional processes within shallow deposits in response to change in sea level and sediment supply (Suter and Berryhill, 1985; Shipp, 1993). Using 2D seismic lines, Prather et al. (1995) studied the seismic facies in the Gulf of Mexico minibasins, which resulted in the identification of the following facies: Convergent Thinning(Ct), Convergent Baselapping (Cb), Draping (D) and Chaotic facies. Using petrophysical data, Prather et al. (1995) found Cb facies to have high sand/shale ratio. The relation between these facies and salt subsidence was addressed in detail by Zoltan et al. (2015) by modeling. However, pattern recognition algorithms such as artificial neural networks have not been widely used in facies classification in intraslope minibasins.

Pattern recognition algorithms are used routinely today by many industries to help recognize trends in large size data. Before pattern recognition algorithms integration in seismic interpretation, seismic facies representing features of interest like channels, reefs, and mass transport complexes were interpreted manually on 2D lines by looking at waveform, phase, frequency, amplitude, and geometric configurations. Introduction of 3D seismic data and proliferation of seismic attributes renders manual interpretation burdensome; for that matter, pattern recognition algorithms were introduced to facilitate facies classification (Zhao et al., 2015).

Starting from simple attributes crossplotting, there are many classification techniques such as *k*-mean, fuzzy clustering, self-organizing maps (SOMs) and artificial neural network (ANN); such algorithms are common to most interpretation packages. ANN have wide use in exploration and production producers such as seismic inversion, waveform recognition and reservoir characterization. Recently, ANN has been applied in facies classification using seismic attributes.

This work applies an unsupervised neural network facies classification to preselected seismic attributes. The classification results, along with minibasin models from previous studies, will be helpful to identify the main seismic facies and predict sand distribution in a minibasin in the study area.

Data

This study analyzes 3D WATS (Wide Azimuth Towed Streamer) seismic data. The WATS geometry follows the same traditional acquisition pattern (in straight parallel lines), but with at least two source vessels placed behind and beside the towed streamer respectively.

The WATS Geometry has many advantages such as increasing coverage for full azimuth offset, low coherent noise, higher resolution, multiple attenuation, and improved reflector continuity especially for those below the salt (Buia et.al., 2008).

The survey was in the Gulf of Mexico within the Garden Banks and the Keathley Canyon protraction. We have 144 km^2 out of the total area of 13542.6 km^2 (Figure 1). The survey was carried out to explore the sub-salt lower tertiary Wilcox formation.

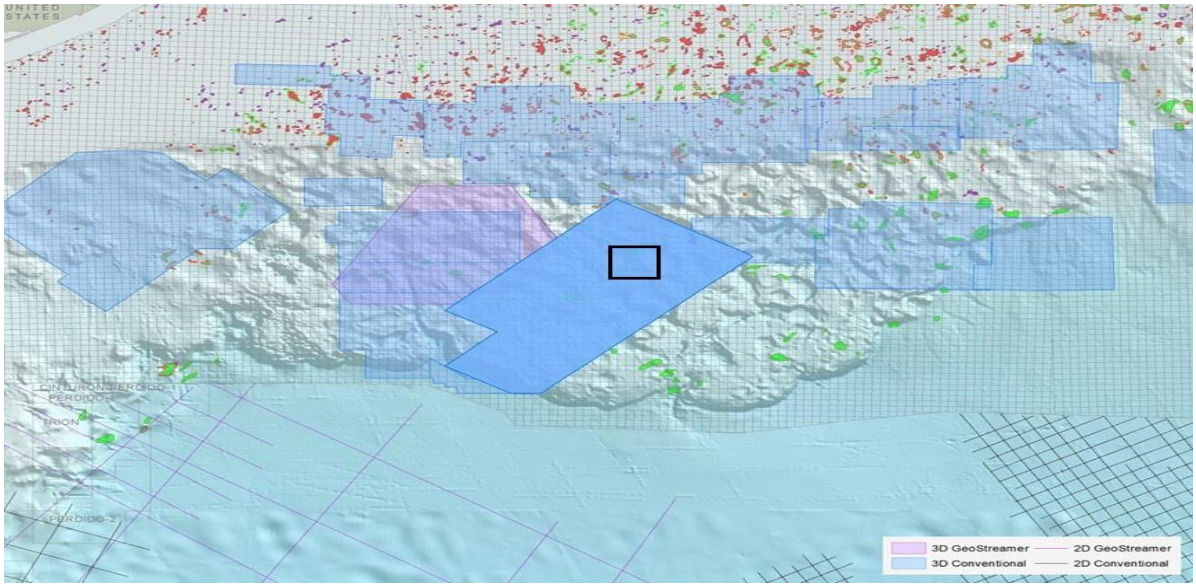

Figure 1: Base map showing the wide azimuth towed streamer (WATS) survey completed by PGS, highlighted by dark blue; the black box approximately outlines the study area. The data is located on the outer continental shelf within the tabular salt and minibasin province of the Gulf of Mexico (GOM) (https://www.pgs.com/data-library/north-and-south-america/gulf-of-mexico/crystal-wats-a--b/).

The survey began in 2006 and the data was fully processed and made available in 2007. The survey was in the NE/SW direction with 10 streamers used in the survey; the streamers were 8100 meters long and 12 meters apart. The source was activated every 37.5 meters; the record length was 14000 milliseconds with a sample rate of 2 milliseconds. The 108-fold data set has a bin size of 15×6.25 meters for acquisition and 30×30 meters for processing. Processing steps including: anomalous amplitude attenuation, water velocity correction, seismic migration, high resolution sediment and salt flooding were applied for better imaging

and improved signal to noise ratio. The final data products are: 1) 3D Kirchhoff prestack depth migrated, 2) wave equation prestack depth migrated, 3) beam migrated sets and, 4) a velocity model.

Methods

The data were first uploaded into Petrel with preset parameters such as geographic coordinates, number of inlines/crosslines and number of samples per trace. Seafloor (SF), top of salt (TOS), base of salt (BOS) and formation tops (FT) were picked through the entire study area with the aid of high precision 3D auto-tracking; manual picking was required in areas with low resolution and high noise. TOS was distinguished as a very bright reflection on top of chaotic zone with very low internal reflection. Since a zero-phase wavelet was used according to North American polarity, SF and TOS were taken as a peak and BOS as a trough. Sand beds were picked at well KC 102 and extrapolated outwards. Faults were also interpreted in highly deformed areas.

Volume attributes of different categories including signal processing, complex trace analysis, structural and stratigraphic attributes were applied to the seismic data. Careful choice of input volume attributes is crucial to build a good quality classification. A better choice of attributes is insured by attributes crossplotting and Correlation Analysis (CA). Attributes that show better clustering on crossplots are the input of correlation analysis for quality check. It is important to apply a Principle Component Analysis (PCA) on the correlated attributes to reduce dimensionality of the input attributes by defining the most important Eigenvectors and their contribution.

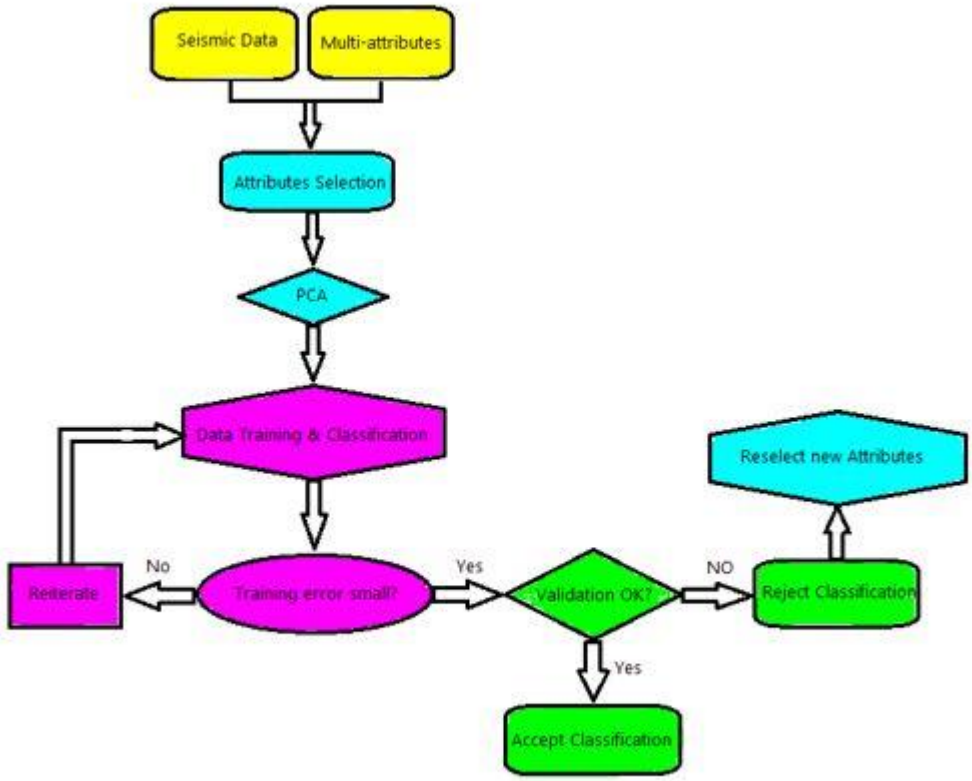

Figure 2: Workflow for unsupervised ANN.

Facies classification is achievable by running an Artificial Neural Network (ANN) Algorithm called Train and Estimation, available in Petrel under utilities. ANN is a human brain like processing algorithm that learns by trial and error using a set of multiple input attributes. There are supervised and unsupervised adaptive networks in Petrel. Supervised Neural Network Analysis is possible when there are training data such as well logs; errors are estimated by comparing computed data to training data. Unsupervised Neural Network analysis is applied when training data are not included in computation; the final output is the result of a probabilistic classification of input attributes. The Competitive Learning Algorithm self organizes the user defined classes; the number of classes is defined by the eigenvectors

identified by the PCA. Petrophysical data are used after the classification process to calibrate the defined classes.

Seismic Attributes Analysis

Root Mean Square (RMS) amplitude is the root mean square of the trace amplitude. RMS is a statistical method that proves useful with sinusoidal data with positive and negative values such as seismic traces. RMS emphasizes acoustic impedance variation which makes it a good indicator of the energy content of the seismic trace. The RMS is computed across a moving window with N number of samples. It is computed according to the following equation:

$$A_{RMS}(t) \equiv \sqrt{\frac{1}{N}\sum_{k=-N/2}^{N/2}\left(f(t+k)\right)^2} \quad \text{.....(1)}$$

$A_{RMS}(t)$: Root mean square amplitude at time *t*.

f (t): The recorded seismic trace.

k: Sample interval.

N: Number of samples.

Figure 2 illustrates the original seismic and its correspondent RMS amplitude section. RMS is very sensitive to amplitude variation. High values of amplitudes are boosted, as indicated on the RMS section, because they are squared before being averaged; they are indicative of high energy content. Low to moderate RMS values dominate the section except for the sea floor due to the large contrast with water acoustic impedance.

Envelope or *Reflection Strength* is defined by Taner et al., (1979), as the combined instantaneous energy of the real and imaginary parts of the complex trace or the modulus of the complex trace which is phase independent. The envelope is computed according to the

following equation:

$$\left|F_{HI}(t)\right| = \sqrt{f^{2}(t) + f^{*2}(t)} \quad \text{.....(2)}$$

$|F_{HI}(t)|$: Envelope or the magnitude of the total instantaneous energy

$f(t)$: Real instantaneous energy at time t.

$f^{*}(t)$: Imaginary instantaneous energy at time t which is the Hilbert transform of $f(t)$.

Figure 2 illustrates the original seismic section and its correspondent envelope displayed in brown red and yellow color scale. High values are highlighted in yellow which correspond to anomalous bright amplitudes on seismic section. Seismic packages with different amplitudes are better separated on the envelope section because it is related to energy content of the seismic trace regardless of the phase. The envelope is mainly used to highlight subtle and major lithologic variations. In major cases, high values of envelope are related to sequence boundaries and gas accumulation (Taner et al., 1979).

Dominant Frequency (DF) represent the RMS frequency of the amplitude spectrum. DF is computed according to equation 3

$$\omega_{RMS} = \sqrt{\omega_{B}^{2} + \omega_{c}^{2}} \quad \text{.....(3)}$$

ω_{RMS}: Root mean square frequency or the centroid of the second moment of the power spectrum.

ω_{B}: Instantaneous bandwidth.

ω_{C}: Instantaneous frequency.

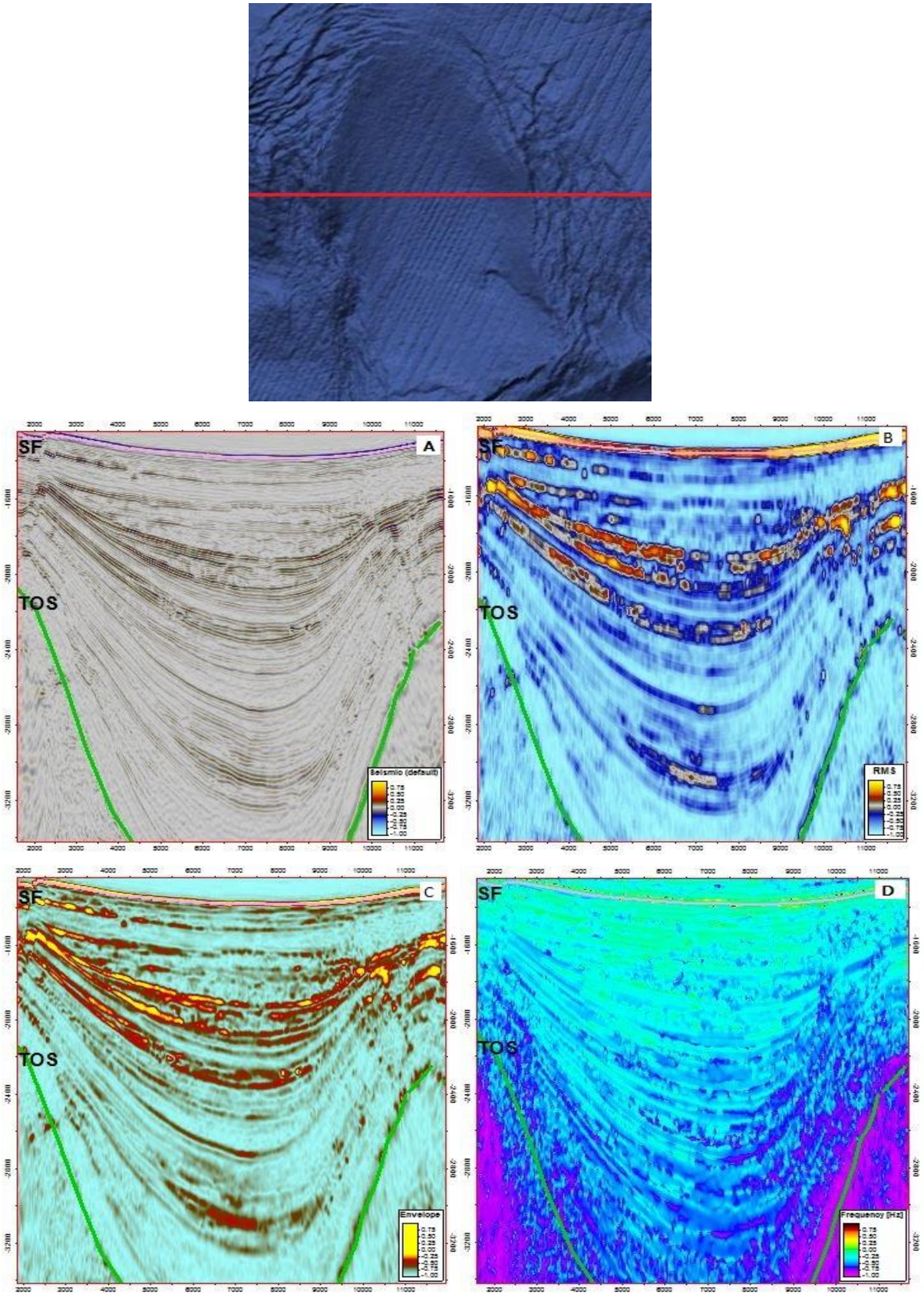

Figure 3: Inline 2387 crosssection through the mininbasin illustrating (a) original seismic section, (b) RMS amplitude, (C) envelope, (D) dominant frequency. Important reflectors such as the sea floor and top of salt are annotated. Color scale bars are displayed at the lower right corner of each section.

Figure 2 illustrates the original seismic section and its correspondent Dominant frequency section. The dominant frequency helps separate salt bodies from other stratigraphy, low values indicate salt uplifting surrounding sedimentation. The power spectrum is very useful to detect frequency shadows that are potential hydrocarbon reservoirs; they are also useful to distinguish channels and salt bodies (Leonardo, 2009).

Attributes Crossplotting

Attributes crossplotting could be implemented in many interpretation softwares where two or more attributes could be crossplotted. The clusters become easily visualized and contoured on crossplots; however, clusters identification becomes burdensome when more than three attributes are crossplotted. From the attributes that enhance lithologic and stratigraphic variation, I choose RMS amplitude, envelope and dominant frequency. Each of these attributes was plotted against the other two. The crossplotts show good clustering except for RMS amplitude versus envelope which correlate linearly.

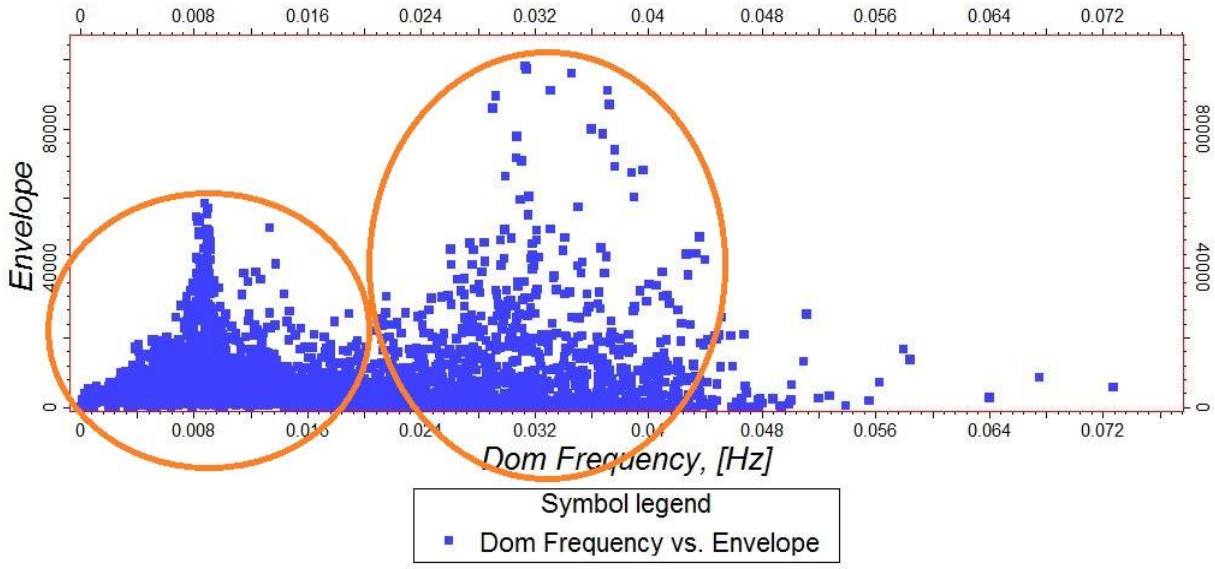

Figure 4: Crossplot of envelope versus dominant frequency. There are 2 major clusters with some outliers. The points in the second cluster are more spread out then the first cluster that has a spiking character. Therefore, both attributes are selected for facies classification.

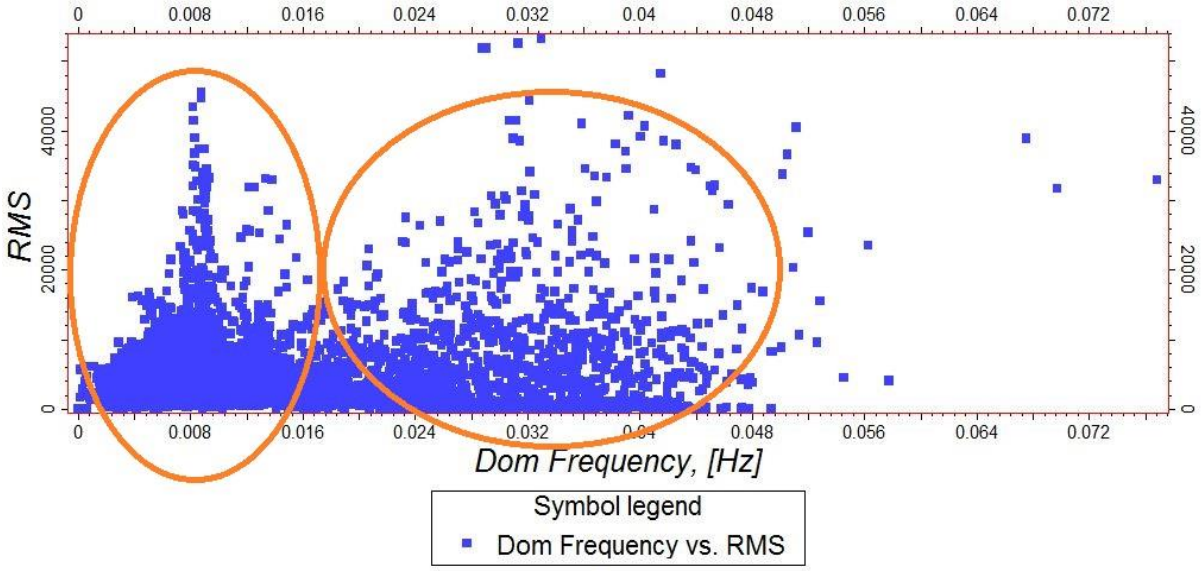

Figure 5: Crossplot of RMS amplitude versus dominant frequency. There are 2 major clusters with some outliers. The clusters show similar characteristics as in envelope versus dominant frequency. Therefore, both attributes are selected for facies classification.

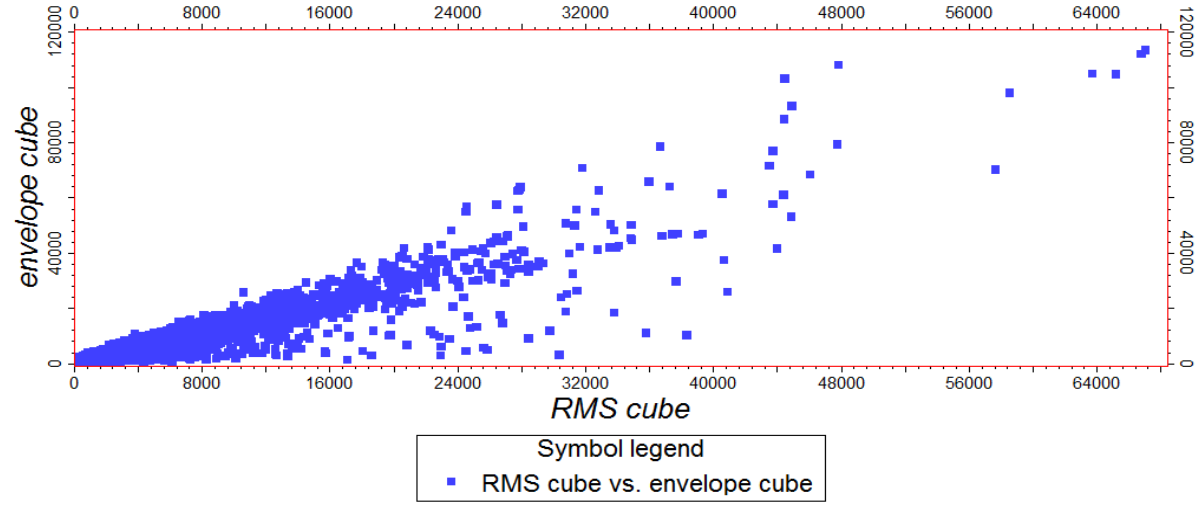

Figure 6: Crossplot of envelope versus RMS amplitude. The plot shows a high correlation because both attributes are related to the energy content of the seismic trace, and they both emphasize the high-energy content of the seismic data.

Correlation Analysis

Correlation analysis results of the selected attributes are displayed in table 1. The correlation coefficients are color coded with values between 0 and 1. The attributes desired for NNA are colored in green with correlation coefficient less than 0.35. Higher values are

highlighted in red as in the case of RMS amplitude with envelope with a correlation coefficient of 0.94. RMS amplitude and envelope attributes could be used together in the classification because both emphasize the high-energy content of the seismic data. Gray cells represent perfect matching as in the case of an attribute with itself.

	Rms	Envelope	Dom frequency
Rms	1.0000	0.9423	0.3120
Envelope	0.9423	1.0000	0.2366
Dom frequenc	0.3120	0.2366	1.0000
Total	0.9467	0.9442	0.3560

Table 1: Correlation analysis result. Desired attributes for classification are those with correlation coefficient lower than 0.5 which means there is less the 50% similarity between them. Highly correlated attributes with correlation coefficient greater than 0.5 are represented by red sells which are again RMS amplitude and envelope.

Principle Component Analysis

Principle component analysis is a linear multivariable technique that helps reduce the dimensionality of the data (Gurney, 1997). The data matrix could be decomposed into its component Eigenvector and Eigenvalue (Mari et al., 1999). The first principle component is obtained by projecting the N-dimensional data against the first eigenvector at each voxel. The second principle component is obtained similarly by projecting either original data or residual data against the second eigenvector; residual data is what left after subtracting the original data from the first eigenvector scaled by the first principle component; The second eigenvector is the vector that best represents the attribute patterns in this residual. The process continues till there are N principle components for all N-dimensions. PCA helps reduce redundant attributes into ‘‘meta attributes’’ to simplify computation (Zhao et al., 2015) and to avoid the risk of losing information as in the case of manual clipping (Linari et al., 2003). PCA results are displayed in Table 2 with eigenvalues ordered from highest to lowest

depending on the importance of the Principle Component (PC). The first principle component has an eigenvalue of 2.08 with 69.39% contribution. The second component has eigenvalues of 0.86 with 28.80% contribution. The last component has an eigenvalue of 0.0544 with the least contribution of 1.81%.

Correlation Coefficients	PC1	PC2	PC3
Rms	0.9692	0.1812	0.1667
Envelope	0.9510	0.2629	-0.1625
Dom frequency	0.4876	-0.8730	-0.0143
Eigenvalue	2.0816	0.8640	0.0544
Contribution (%)	69.39	28.80	1.81
Cumulative Contribution (%)	69.39	98.19	100.00

Table 2: Principle components with their eigenvalues and overall contributions. These principle components are eigenvectors that best represent the data matrices, and that are scaled by eigenvalues. The components are classified from highest to lowest depending on their contribution.

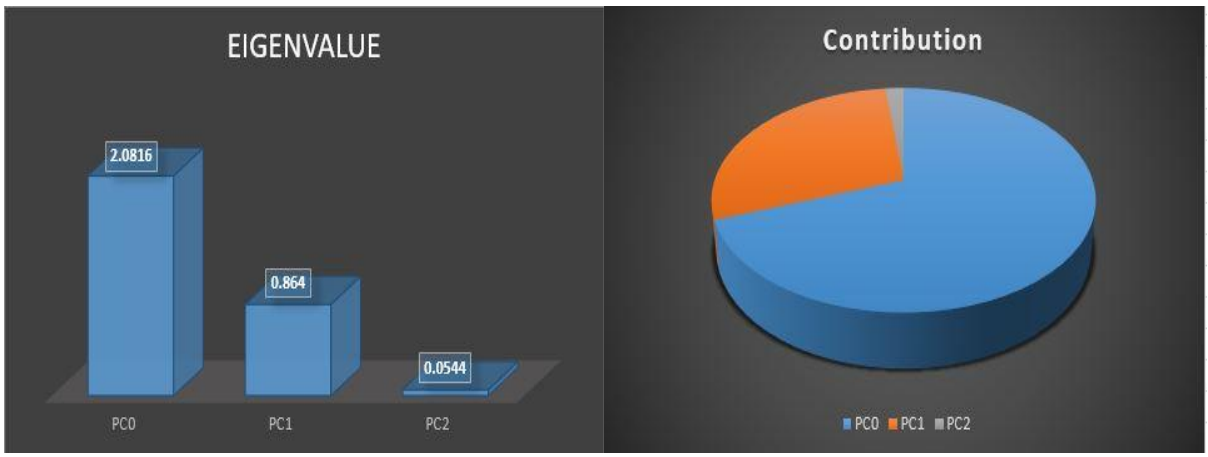

(a) (b)

Figure 7: Graphic representation of (a) Principle Components Eigenvalues, (b) Contribution pie chart. The first principle component has the highest eigenvalue which contributes about two thirds. The second principle component contributes about one third. The third principle component has the least contribution.

Data Training and Classification

Automatic facies classifications and their use in seismic interpretation were discussed before by Coleou et al., (2003) and Linari, et al., (2003). They aim to identify variations not

easily observed on seismic data that may ultimately correspond to geologic variations obscured by noise and processing artifacts. Each data point is given a value and correlated with the class that best fits in. The classification is based on a feed-forward artificial neural network. Many iterations are applied until the maximum errors of 10% is reached. Final validation with wireline logs decides whether the classification results are acceptable or new attributes should be selected. The final model is a cube with three facies classes that better represent facies classes identified within the intraslope minibasin in the study area.

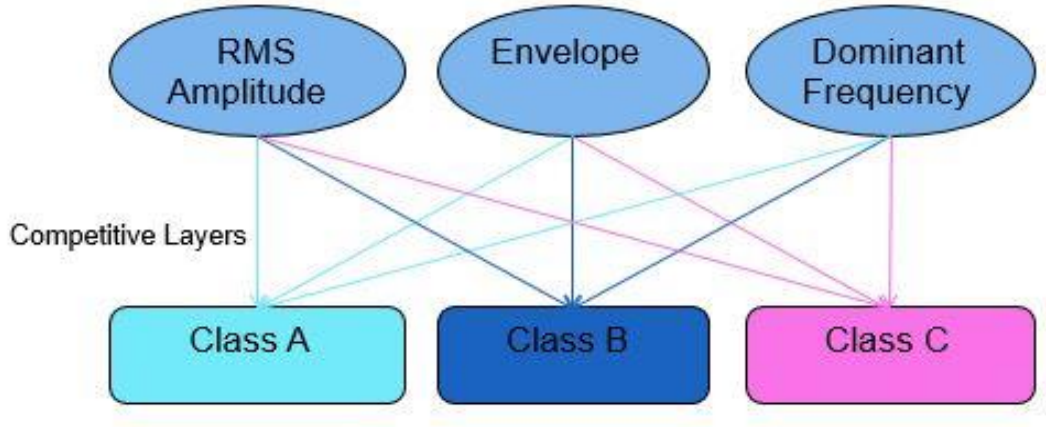

Figure 8: The attributes used in the classification are: RMS amplitude, envelope and dominant frequency. The competitive learning algorithm self organizes the user defined number of classes. In the learning process, the central points of each class are distributed randomly, and then adjusted to fit the center of each class. There were 20 iterations with the maximum error of 10%.

Facies Succession:

The result of the classification is a cube with 3 seismic facies classes. The facies classes were calibrated with Gamma Ray log from well KC102 to give the facies their lithological significance. The original seismic data was also used in the interpretation process to establish a correspondence between seismic texture and lithology: Class A is associated with low amplitudes that lack internal reflections, and they are mostly correlated with shale

rich intervals; Class B is correlated with sand rich intervals, and on the original seismic data they correspond to high amplitude reflections; Class C correspond to chaotic seismic character on seismic data that represent salt.

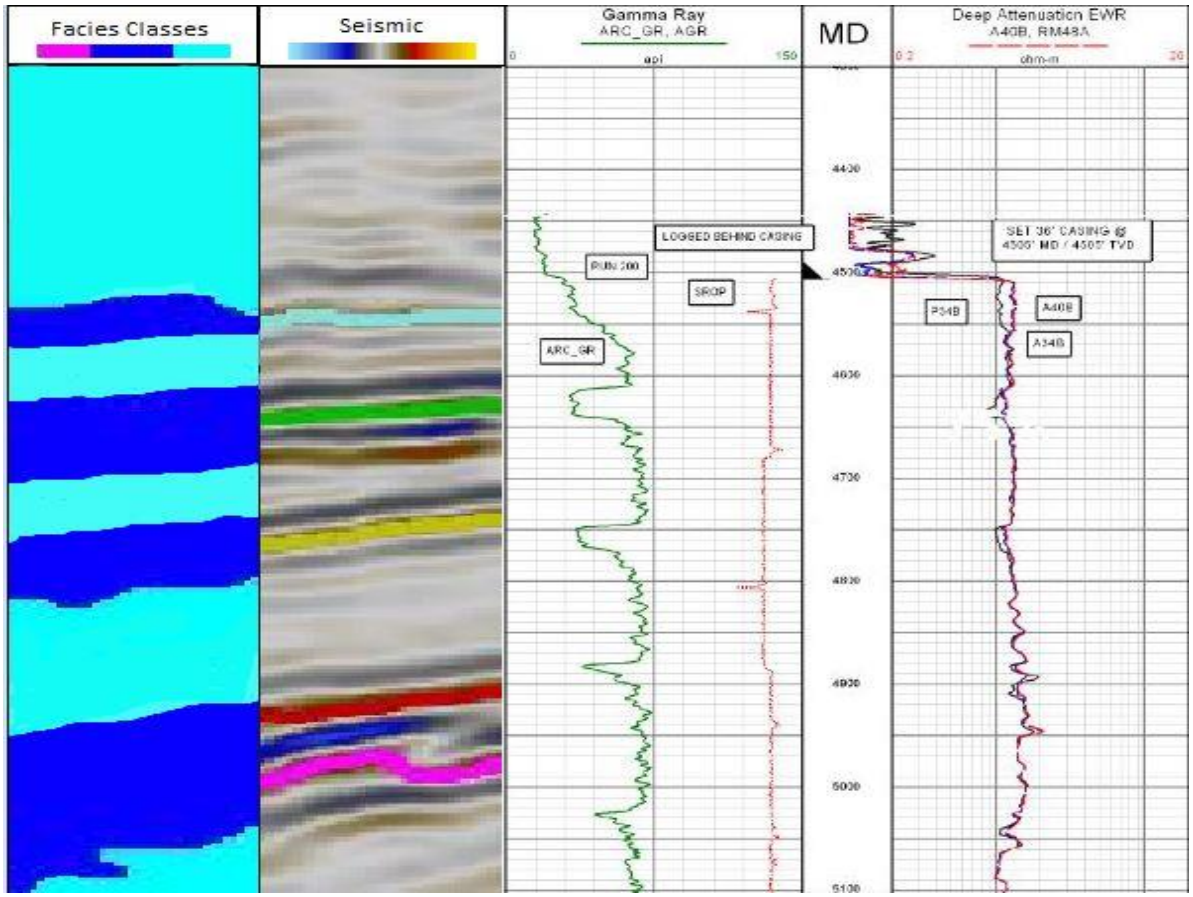

Figure 9: Sand beds were picked at well kc102 using the gamma ray log; the sand line was at 50 API. The blue facies coincide with intervals that contain sand.

The calibrated facies were used to predict the lithology in a minibasin (away from well control) to understand the distribution of sand. Three types of stratal patterns were found within the minbasin in the study area: convergent thinning, convergent baselaping and bypassing facies. To help understand the stratal patterns within intraslope minibasins in response to sediment/subsidence interplay, I used model results from Zoltan Sylvester et al.,

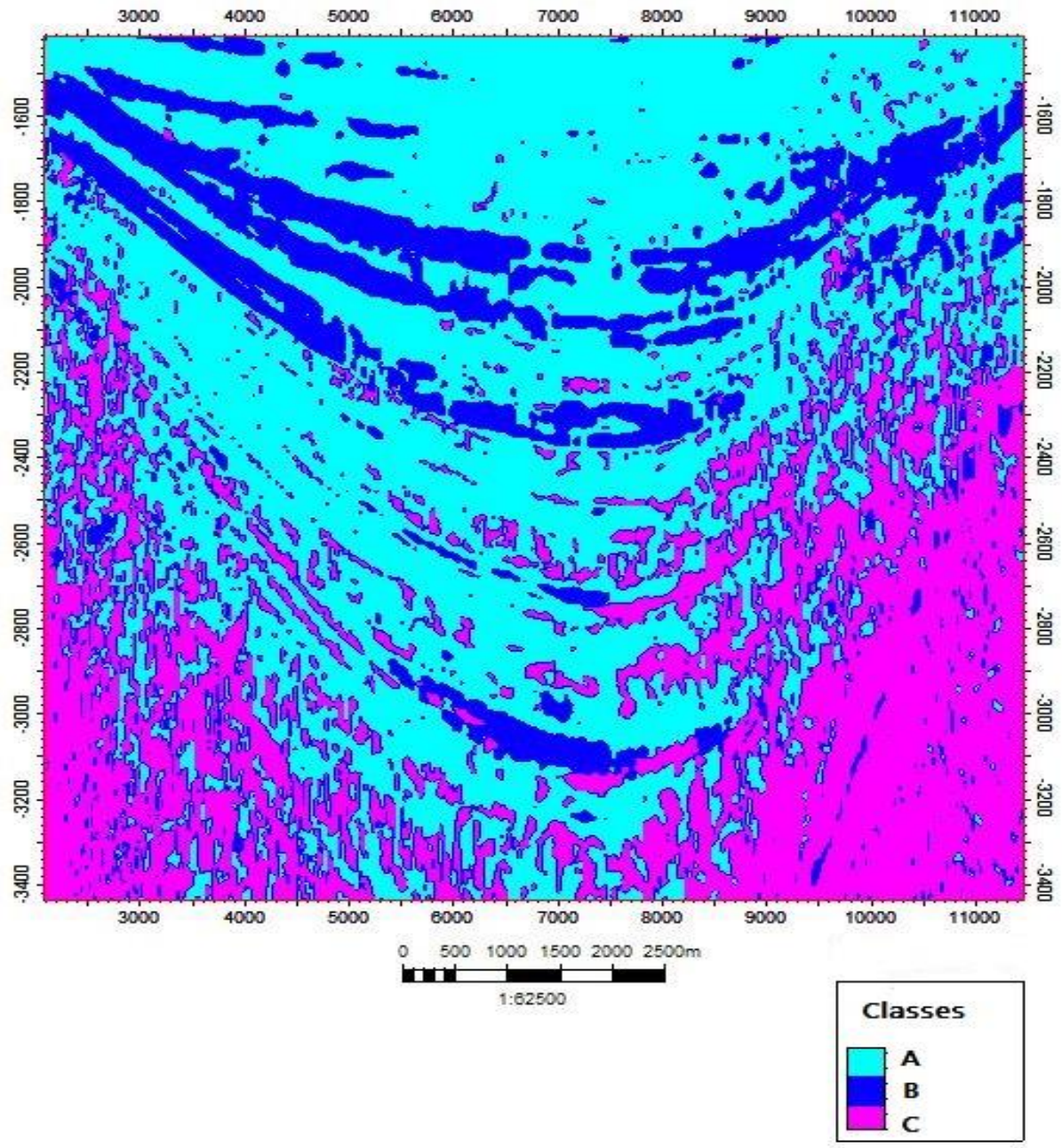

Figure 10: Cross section showing the different facies classes. dark blue class represent the most sand-rich facies. Light blue represents shale-rich facies. Purple is associated with salt.

(June 2015). They developed a simple model that captures large scale features with concentration on mass balance of the system. The model has many variable input parameters such as the local subsidence and volumetric sediment discharge $\boldsymbol{Q_{in}}$ which is the average sediment volume of each inflow episode; both parameters are from real case studies in the Gulf of Mexico, and measured in (volume/time). Background sedimentation rate ***bg*** account

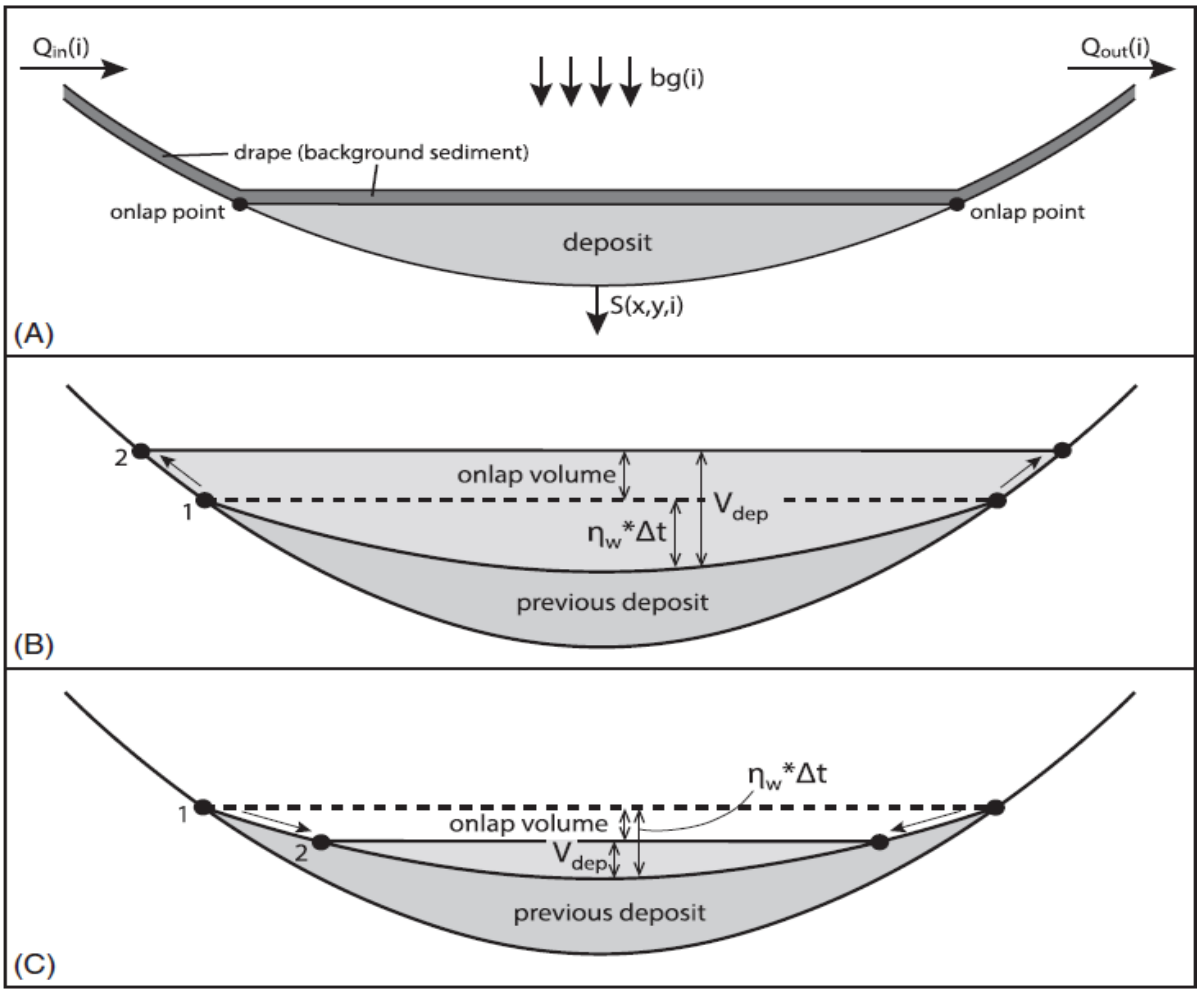

Figure 11: (A) sketch that simplifies the main parameters and terminology for simple model. stratal point termination location are the result of the interplay between volume of sedimentation and volume of subsidence: if volume of sedimentation exceeds the volume made through subsidence, there would be an onlap at the basin flank (B); if opposite, an offlap would be observed (C) (Zoltan et al., AAPG© 2015). reprinted by permission of the AAPG whose permission is required for further use.

for pelagic and hemipelagic deposits. The outputs of the model are outgoing sediment discharge ***Qout*** which represents the rate of sediment leaving the system, locations of onlap points and volume of accommodation ***Vacc*** which is the volume created through subsidence (Figure 11). Parameters like channelization and erosion are ignored because minibasins are depositional overall; compaction also is ignored because its effect is deemed of second order (Zoltan et al., 2015). Finer details could not be reproduced; the model captures only large scale stratigraphic patterns.

The first case investigates the effect of basin topography on the stratigraphic architecture. They started with a relatively shallow basin topography and constant sediment supply. Because the space occupied by the incoming sediment is recreated by subsidence in each time step; an equilibrium state was reached and the location of onlap points remained the same. Perfect convergence of stratigraphic surfaces was observed on cross section. Such stacking pattern is observed in the lower and middle part of my minibasin; these facies are the equivalent of convergent thinning facies.

In the second scenario, they start with a minibasin with significant depth while keeping the sediment supply and subsidence rate the same. Sedimentation progressively fills the minibasin and the onlap points migrate towards the basin margin. As the basin fills, the onlap point become closer to each other because the deposition surface increases. On seismic section, such patterns are observed in the upper portion of the minibasin. Sedimentation progressively filled the accommodation space created with an onlap staking pattern like in modeling. These seismic facies are the equivalent of the convergent baselaping facies.

The third and fourth scenario investigate sediment supply effect on the stratigraphic architecture by making it sinusoidal which is closer to reality because sediment supply in minibasins experience fluctuation as feeder channels are abandoned or reactivated. Subsidence rate was kept constant. The fourth case consider bypass in case of doubling sediment input which periodically outpace accommodation. The final model results are three stratigraphic packages (three cycles of sediment input). The packages are separated by onlap

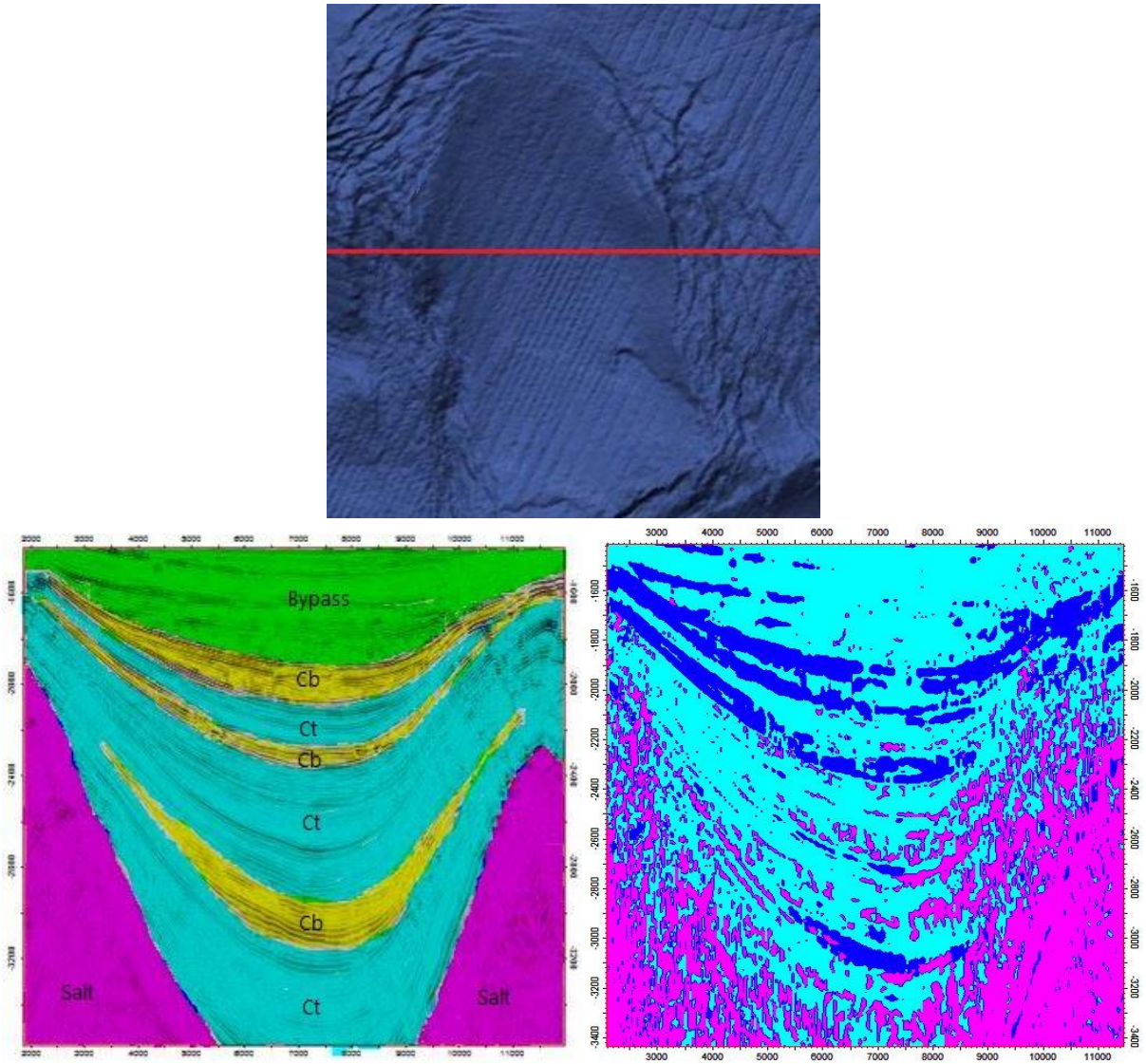

(a) (b)

Figure 12: (a) Original cross section through the minibasin with seismic facies delineated. (b) correspondent cross section through ANN facies classification cube. The stacking pattern of seismic facies is like those found by modeling. Ct, Cb and bypass facies are present except for offlaping facies that are hard to observe on seismic section. On the classification section, the dark blue facies are associated with sand rich intervals which coincide with Cb facies on seismic section.

and offlap surfaces. The bypass packages have a chaotic convergent character that terminate at the basin edge. This kind of stratigraphic succession is observed in the upper portion of the minibasin in the study area. Such successions are also observed in the Gulf of Mexico within well-known minibasins like the Auger basin (Booth et al., 2003) and Mars basins (Meckel et

al., 2002).

Application to an Intraslope Minibasin in the Keathely Canyon

The minibasin in the study area has a Gaussian cross section; it shows stratigraphic patterns with variable degrees of convergence and onlap similar to those found by modeling. Although the minibasin has a significant depth, it was effected by bypass. The lower packages show a high degree of convergence and lack of onlapping geometries in contrast with upper packages where onlap is observed at the basin edge. These facies are the equivalent of Ct and Cb observed by Prather et al. (1998). They are the result of: (1) ongoing subsidence during sedimentation, (2) intermittent sedimentation (long periods of no significant siliciclastic input interrupted by relatively short phases of high sediment flux) and (3) periods of high sediment flux (Zoltan et al., 2015). Chaotic seismic facies on top of high intensity line in the upper portion of the manibasin correspond to bypass facies assemblage; their presence could be explained by a decline in subsidence rate or large sediment influx that outpaced the creation accommodation space.

Most of the slope basin-fill deposits in the GOM are turbidite lobes, channels and mass transport complexes. These deposits are widespread and contain sand and shale that extend laterally within minibasins (Reilly and Flemings, 2010). Classification result shows that Cb facies are most sand rich then other facies such as Ct and bypass facies (Figure 12). Prather et. al. (1998) also found the Cb facies to have high net to gross sand ratio within minibasins in the Gulf of Mexico slope region. In the case of constant subsidence, high sediment supply result in well-defined onlap and limited convergence whereas low sediment supply result in perfect convergence and poorly defined onlap. High sediment supply tends to be more

sand-rich than low sediment supply and that is why Cb facies show high sand content. Sand-rich high sediment supply in deep marine setting could be explained by submarine fans that transport sand from the shelf and upper slope to the middle slope and abyssal fan. Low sediment supply could be explained leveed channel deposits and muddy turbidite that grade into Ct facies. Bypass facies and their chaotic character could be explained by slumps and submarine slides that are the result of slope fail due to progradation above at grade slope.

Conclusion

Unsupervised classification using energy related attributes such as RMS amplitude, envelope and dominant frequency was effective in discriminating sand-rich from shale-rich intervals within the minibasin; it was also effective for modeling the salt in the study area.

The basin fill in the study area is composed of alternating Ct and Cb facies. The basin initial topography and sediment supply are the major factors that shape those facies in the case of constant subsidence rate. The bypass facies found at the upper portion of the minibasin are controlled by sediment supply or subsidence rate.

Unsupervised classification was useful to predict the lithology in the minibasin distal from well control where Cb facies were found to be the most sand rich.

Recommendations

Unsupervised classification could be the first approach to predict the lithology within minibasin environment. Supervised classification guided by well logs would better estimate the physical properties between wells based on the petrophysical data available.

The use of additional edge detection attributes like coherency would improve separation of salt from other stratigraphy.

References

Barnes, A. E., and K. J. Laughlin, 2002, Investigation of methods for unsupervised classification of seismic data: 72nd Annual International Meeting, SEG, Expanded Abstracts, 2221–2224.

Booth, J. R., M. C. Dean, A. E. DuVernay III, and M. J. Styzen, 2003, Paleo-bathymetric controls on the stratigraphic architecture and reservoir development of confined fans in the Auger Basin: Central Gulf of Mexico slope: Marine and Petroleum Geology, v. 20, no. 6, p. 563–586.

Boyd, J. D., M. J. Mayall, and C. A. Yeilding, 1993, Depositional models for intraslope basins: variability and controls (abs.): AAPG Annual Meeting Program with Abstracts, p. 85.

Buia, M., Hill, D., Houbiers, M., Laura, S., Menlikli, C., Moldoveanu, N., Snyder, E. (2008). Shooting Seismic in Circles. Oilfield Review, Autumn, 18 – 31.

Chopra, S., Marfurt, K. J. (2007). Seismic attributes – A historical perspective. Geophysics, Vol.70; No.5, 3SO - 28SO.

Coleou T., Poupon, M. and Azbel, K., 2003. Unsupervised seismic facies classification: A review and comparison of techniques and implementation. Interpreter's corner, The Leading Edge, October 2003, 942-953.

Diegel, F. A., J. F. Karlo, D. C. Schuster, R. C. Shoup, and P. R. Tauvers, 1995, Cenozoic structural evolution and tectonostratigraphic framework of the northern Gulf Coast continental margin, *in* M. P. A. Jackson, D. G. Roberts, and S. Snelson, eds., Salt tectonics: a global perspective: AAPG Memoir 65, p. 109–151.

Farzadi, P., 2006. Seismic facies analysis based on 3D multi-atttibute volume classification, Daryan formation, SE Persian Gulf. Journal of Petroleum Geology, Vol. 29(2), April 2006, pp 159 - 174Fehmers, G., Hocker, C. (2003). Fast structural interpretation with structure-oriented filtering. Geophysics, Vol. 68, No. 4, 1286 – 1293.

Gurney, K., 1997. An introduction to neural networks. UCL Press, 234p.
Hudec, M., and M. P. A. Jackson, 2007, Terra infirma: Understanding salt tectonics: Earth Science Reviews, v. 82, no. 1–2, p. 1–28.

Hudec, M.R., Jackson, M.P.A., Schultz-Ela, D.D., 2009. The paradox of minibasin subsidence into salt: clues to the evolution of crustal basins. Geol. Soc. Am. Bull. 121,

201–221.

Kendrick, J. W., 2000, Turbidite reservoir architecture in the Northern Gulf of Mexico deepwater: Insights from the development of Auger, Tahoe, and Ram/Powell Fields: Gulf Coast Section-SEPM Foundation 20th Annual Research Conference, Houston, Texas, December 3–6, 2000, p. 450–468.

Lee, G. H., J. S. Watkins, and W. R. Bryant, 1996, Bryant Canyon fan system: an unconfined, large river-source system in the northwestern Gulf of Mexico: AAPG Bulletin, v. 80, no. 3, p. 340–358.

Linari, V., Santiago, M., Pastore, C., Azbel, K. and Poupon, M., 2003. Seismic facies analysis based on 3D multi-attribute volume classification, La Palma field, Maracaibo, Venezuela. The Leading Edge, January 2003, 3236.

Leonardo, A., 2009.Seismic Attributes in Hydrocarbon Reservoirs Characterization. Master thesis, Department of Geoscienses, University of Aveiro.

Mahaffie, M. J., 1994, Reservoir classification for turbidite intervals at the Mars discovery, Mississippi Canyon 807, Gulf of Mexico: Submarine fans and turbidite systems: Gulf Coast Section-SEPM Foundation 15th Annual Research Conference, December 4–7, 1994, p. 233–244.

Mari, J.L., Glangeaud, F., and Coppens, F., 1999. Signal processing for geologists and geophysicists. Institut francais du pétrole, 458pp.

McGee, D. T., P. W. Bilinski, P. S. Gary, D. S. Pfeiffer, and J. L. Sheiman, 1993, Geologic models and reservoir geometries of Auger field, deepwater Gulf of Mexico, *in* P. Weimer, A. H. Bouma, and B. F. Perkins, eds., Submarine fans and turbidite systems—sequence stratigraphy, reservoir architecture, and production characteristics: GCAGS Fifteenth Annual Research Conference, p. 245–256.

Meckel III, L. D., G. A. Ugueto, D. H. Lynch, and B. M. Hewett, 2002, Genetic stratigraphy, stratigraphic architecture, and reservoir stacking patterns of the upper Miocene–lower Pliocene greater Mars-Ursa intraslope basin, Mississippi Canyon, Gulf of Mexico: Gulf Coast Section-SEPM Foundation 22nd Annual ResearchConference, Houston, Texas, December 8–11, 2002, p. 113–147.

Peel, F. J., 2014, How do salt withdrawal minibasins form? Insights from forward modeling, and implications for hydrocarbon migration: Tectonophysics, v. 630, p. 222–235.

Pilcher, R. S., B. Kilsdonk, and J. Trude, 2011, Primary basins and their boundaries in the deep-water northern Gulf of Mexico: Origin, trap types, and petroleum system implications:

AAPG Bulletin, v. 95, no. 2, p. 219–240.

Prather, B.E., Booth, J.R., Steffens, G.S., Craig, P.A., 1998. Classification, lithologic calibration, and stratigraphic succession of seismic facies of intraslope basins, deep water Gulf of Mexico. AAPG Bull. 82 (5a), 701e728.

Prather, B. E., J. R. Booth, G. S. Steffens, and P. A. Craig, 1995, Classification and stratigraphic succession of seismic facies in intraslope basins, deep-water Gulf of Mexico, U.S.A. (abs.): AAPG Annual Meeting Program with Abstracts, p. 77A.

Reilly, M. J., and P. B. Flemings, 2010, Deep pore pressures and seafloor venting in the Auger Basin, Gulf of Mexico: Basin Research, v. 22, no. 4, p. 380–397.

Robinson, E. A., Durrani, T. S., Peardon, L. (1986). Geophysical Signal Processing. Prentice – Hall, 1 – 25.

Satinder, C. Kurt J. M. (2007). Seismic attributes for prospect identification and reservoir characterization. SEG Geophysical Development Series No. 11.

Satterfield, W. M., and E. W. Behrens, 1990, A late Quaternary canyon/channel system, northwest Gulf of Mexico continental slope: Marine Geology, v. 92, no. 1–2,
p. 51–67, doi:10.1016/0025-3227(90)90026-G.

Shipp, R. C., 1993, Late Pleistocene Mississippi River canyons: slope turbidite systems in western Mississippi Canyon and Atwater, northern Gulf of Mexico (abs.): AAPG Annual Meeting Program with Abstracts, p. 182.

Steffens, G. S., 1993, Gulf of Mexico deep water seismic stratigraphy (abs.): AAPG Annual Meeting Program with Abstracts, p. 186.

Suter, J. R., and H. L. Berryhill, Jr., 1985, Late Quaternary shelfmargin deltas, northwest Gulf of Mexico: AAPG Bulletin, v. 69, p. 77–91.

Taner, M. T., Koehler, F., Sheriff, R. E. (1979). Complex Seismic trace analysis. Geophysics, Vol.44; No.6, 1041-1063.

T. Zhao, V. Jayaram, A. Roy, and K. J. Marfurt, A comparison of classification techniques for seismic facies recognition. SEG Interpretation, Vol. 3, No. 4 (November 2015); p. SAE29–SAE58.

Zoltán, S., Alessandro, C., Carlos, P. (2015). Stratigraphic evolution of intraslope minibasins: Insights from surface-based model. AAPG Bulletin, v. 99, no. 6, pp. 1099–1129.

Vita

The author was born in Mila, Algeria in 1986. He graduated from Houari Boumedian high school in 2003. The author immediately joined University of Jijel for three years to complete the core courses for earth science degree, and then transferred to University of Constantine to complete two years of specialty in hydrogeology to obtain an engineering degree in 2008. It was at the university of Constantine that he discovered his passion for geophysics, and decided to move to USA to peruse his studies. He was accepted for master program in the earth and environmental science department of University of New Orleans in 2013 to became a member of geophysical research team.